International Geology Review, Vol. 48, 2006, p. 778–790.

P-T Path for Ultrahigh-Pressure Garnet Ultramafic Rocks of the Cuaba Gneiss, Rio San Juan Complex, Dominican Republic

RICHARD N. ABBOTT, JR.,[1]
Department of Geology, Appalachian State University, Boone, North Carolina 28608

GRENVILLE DRAPER,
Department of Earth Sciences, Florida International University, Miami, Florida 33199

AND BONNIE N. BROMAN
Department of Geology, Appalachian State University, Boone, North Carolina 28608

Abstract

Ultrahigh-pressure (UHP) rocks in the Cuaba Gneiss include Grt ultramafic rocks, mafic eclogite, and partially retrograded equivalents. The Grt ultramafic rocks (Spl-bearing Grt peridotite, Spl-bearing Grt clinopyroxenite, Crn-Spl–bearing Grt clinopyroxenite) are of igneous origin, with magmatic conditions of P > 3.5 GPa, T > 1550°C. The magmatic history took place in the asthenosphere. New chemical analyses of minerals give the following subsolidus conditions: Grt peridotite, 3.0–4.2 GPa, 838-867°C; Grt clinopyroxenite (Grt + Cpx + Spl + Crn), 2.75 GPa, 807°C. The ultramafic rocks are associated with partially retrograded eclogite, interpreted as deep-subducted oceanic crust. New chemical analyses of minerals in the eclogite give conditions that relate to the retrograde decomposition of Grt + Omp + Qtz to Grt + Pl + Di + Qtz, 1.8 GPa, 730°C.

The P-T path for the Grt ultramafic rocks is modeled in three parts: (1) slow, isobaric (> 4 GPa) cooling in the mantle, >1550°C down to ~850°C; (2) relatively rapid, nearly adiabatic (?) decompression, ~4 GPa (~850°C) down to ~1 GPa (~700°C); and (3) relatively rapid, non-adiabatic decompression and cooling. The first part of the path (1) took place in the mantle above the subduction zone and relates to delivery of the Grt ultramafic rocks to the subduction zone. Incorporation of Grt ultramafic rocks in the deep-subducted oceanic crust (eclogite) marked the end of this part of the path. The second part of the path (2) was associated with transport up the subduction zone. Retrograde P-T conditions for the eclogite fall on this part of the path, supporting the idea that the Grt ultramafic rocks were transported as blocks in the eclogite. The third part of the path (3) relates to final uplift to the surface.

Introduction

THE PURPOSE of this contribution is to develop a P-T path for ultrahigh-pressure (UHP) rocks of the Cuaba Gneiss in the Dominican Republic (Abbott et al., 2001a, 2001b, 2003a, 2003b, 2005a, 2005b; Draper et al., 2002; Broman et al., 2005). Among globally scarce UHP rocks, the Dominican example is unusual in many respects. Grt ultramafic rocks show clear and exciting evidence for magma chamber processes under asthenospheric conditions (P > 3.4 GPa, T > 1550°C; Abbott et al., 2003a, 2005a, 2005b; Broman et al., 2005). Garnet clinopyroxenite shows the only known, natural occurrence of coexisting garnet, spinel and corundum (see Ackermand et al., 1975). The terrane itself was delivered to the surface at an ocean-ocean convergent margin, confounding any simple explanation for uplift.

New chemical analyses of minerals were used to estimate P-T conditions for three principal rock types (Grt peridotite, Crn-bearing Grt clinopyroxenite, and eclogite). The estimated conditions constrain retrograde P-T paths for the Grt ultramafic rocks and associated eclogite. The results are important in developing a tectonic model for (1) assembling the parts of the terrane and (2) delivering the terrane to the surface of the earth.[2]

[1]Corresponding author; email: abbottrn@appstate.edu

[2]Mineral and component abbreviations are consistent with Kretz (1983).

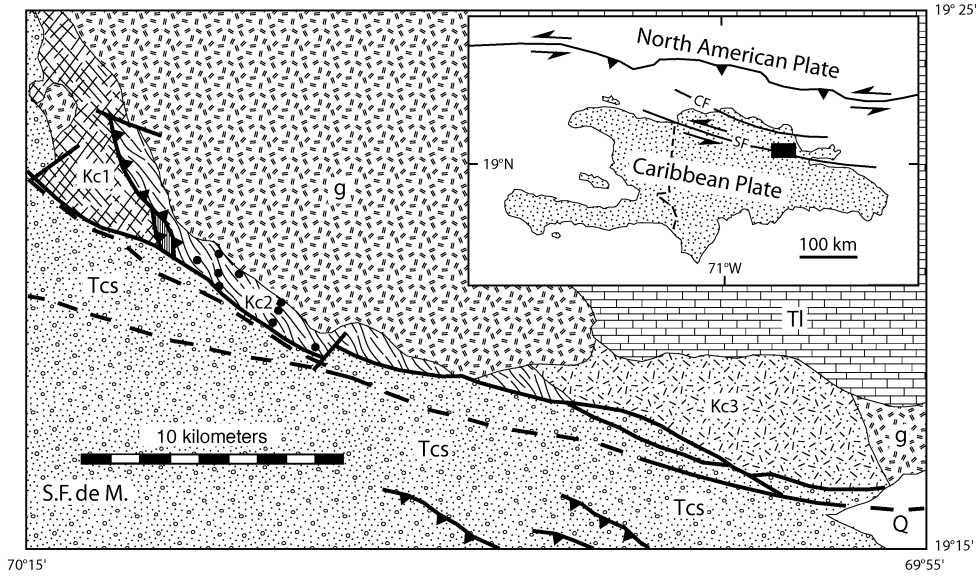

FIG. 1. Geology of the southern part of the Rio San Juan Complex. The Island of Hispaniola is shown in the inset. The vertical dashed boundary separates Haiti (west) from the Dominican Republic (east). The Cordillera Septentrional occupies the land north of the Septentrional fault (SF) in the Dominican Republic. Movement between the North American plate and Caribbean plate is distributed over the Septentrional fault (SF), Camu fault (CF), and an offshore strongly oblique covergent zone (Mann et al., 2002; Jansma et al., 2000). The study area is marked by the filled rectangle. The geologic map shows the southern part of the Cretaceous Rio San Juan Complex (re-mapped 2002–2005, cf. Draper and Nagle, 1991). The Cuaba Gneiss consists of hornblende schist (Kc1), garnet hornblende gneiss (Kc2), garnet metadiorite (Kc3). Small, filled circles in Kc2 represent sites where garnet ultramafic rocks were observed or sampled from boulders. The Cuaba Gneiss is intruded by the Rio Bobo gabbro complex (g). Younger sedimentary rocks and sediment are Upper Eocene–Miocene clastic sedimentary rocks (Tcs), Neogene limestones (Tl), and Quaternary alluvium (Q). Reverse faults: bold, toothed lines (teeth, on hang wall). Left-lateral strike-slip faults: bold un-ornamented lines, dashed where uncertain. S.F. de M. is the city of San Francisco de Macoris.

Geologic Setting

The Dominican Republic occupies the eastern two-thirds of the Island of Hispaniola (Fig. 1). The island is located at the northern edge of the Caribbean plate. Like the other islands of the Greater Antilles (Jamaica, Puerto Rico, southeasternmost Cuba), the basement began as an Early Cretaceous, intra-oceanic island arc complex above a NE-dipping, Pacific-derived plate (Pindell and Barrett, 1990; Draper et al., 1994, 1996; Pindell, 1994; Pindell et al., 2005). In the mid-Cretaceous (~120–100 Ma; Pindell and Barrett, 1990), the plate boundary was relocated from the Pacific side to the Atlantic side of the island-arc complex and the polarity of subduction reversed to the present-day configuration (i.e., SW- to W-dipping subduction, plate boundary on the Atlantic side). From the Late Cretaceous to mid-Eocene, the intra-oceanic island arc widened by accretion, in response to SW-directed subduction of oceanic parts of the North and South American plates (Pindell and Barrett, 1990; Pindell, 1995; Draper et al., 1996; Pindell et al., 2005). The original island-arc system has since been modified by E-W, left-lateral, transcurrent tectonics (Fig. 1) that began in the mid-Eocene and continues today (Mann et al., 1990; Draper et al., 1996). GPS studies indicate that most of the current movement between the North American and Caribbean plates, in the vicinity of the study area, takes place along the Septentrional fault (Jansma et al., 2000; Mann et al., 2002).

The Cordillera Septentrional occupies the land north of the Septentrional fault (Fig. 1) in the Dominican Republic. Upper Eocene to Lower Miocene siliciclastic and carbonate sedimentary rocks cover most of the metamorphic and igneous basement complex (Eberle et al., 1982; Lewis and

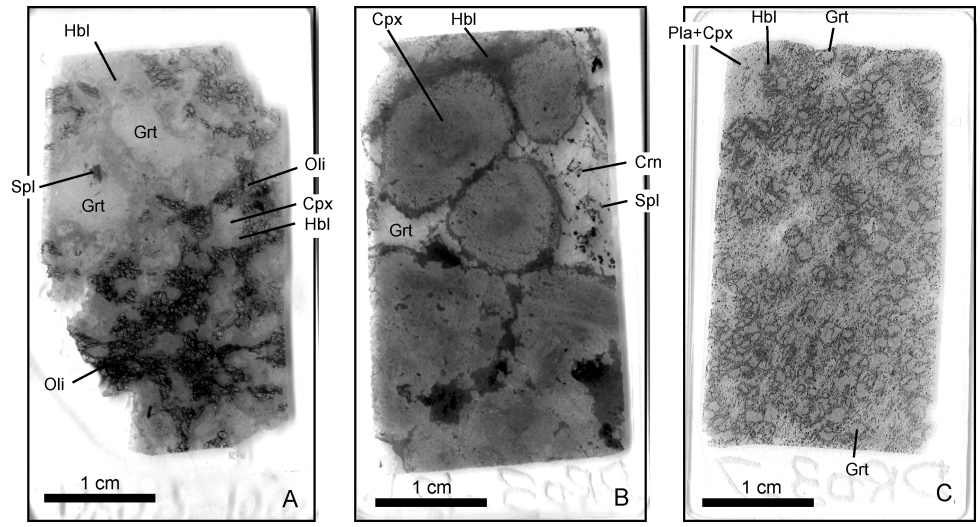

FIG. 2. Digital images of thin sections. A. Garnet peridotite (DR03-10). B. Crn-bearing garnet clinopyroxenite (DR03-12). C. Partially retrograded eclogite (DR03-7).

Draper, 1990). Only locally, where the cover has been eroded away, is the Cretaceous basement exposed in a number of stratigraphic windows, or "inliers." The Cuaba Gneiss (Fig. 1) is the southernmost unit in the largest of these inliers, known as the Rio San Juan Complex (Eberle et al., 1982; Draper and Nagle, 1991). The Cuaba Gneiss unit is approximately 30 km long and up to 6 km wide. On its north side, the Cuaba Gneiss was intruded by gabbroic to quartz dioritic rocks of the Rio Boba Intrusive Complex (Draper and Nagle, 1991). On its southern side the Cuaba Gneiss is faulted against Tertiary siliciclastics.

The Cuaba Gneiss is divided into three members, according to the dominant rock type. From west to east (Fig. 2), the members are hornblende schist (Kc1), garnet hornblende gneiss (Kc2), and garnet metadiorite (Kc3). The common mineral assemblage in all three units is Hbl + Pl (andesine) + Qtz + Rt ± Grt ± Bt ± Ep. The units differ mainly in texture and modal abundance of minerals. Draper and Nagle (1991) suggested a mafic protolith (basalt/diabase/gabbro) of oceanic crustal origin.

This study focuses on minor constituents, garnet ultramafic rocks, and eclogite in the garnet hornblende gneiss (Kc2). Evidence for eclogite is in the form of Pl-Di(symplectite) + Grt, with greater or lesser amounts of hornblende depending on the extent of retrograde hydration (Abbott and Draper, 1998, 2002). The retrograded eclogite occurs as mm- to dm-scale layers in otherwise symplectite-free gneiss. Garnet peridotite and garnet clinopyroxenite (Abbott et al., 2001a, 2003a, 2003b, 2005a, 2005b) occur as stream boulders (up to 4 meters in diameter) eroded out of the hornblende gneiss (Kc2).

Petrography

Details of the petrography of the garnet ultramafic rocks are reported elsewhere (Abbott et al., 2001a, 2001b, 2005a). A summary is given here for examples used in this study. The eclogite is discussed in somewhat more detail, as it has not been described in the context of the present example. The relevant rock types and mineral assemblages are as follows:

Garnet peridotite (DR03-10),
Cpx + Ol + Grt + Spl + hornblende + serpentine

Garnet peridotite (DR00-3), locally on a cm-scale,
Cpx + Grt + Spl + Crn + hornblende

Corundum-bearing garnet clinopyroxenite (DR03-12),
Cpx + Grt + Spl + Crn + hornblende

Eclogite (DR03-7),
Pl-Cpx symplectite + Grt + Qtz + zoisite + hornblende

Accessory minerals include magnetite and pyrite.

Garnet peridotite

Coarse, granoblastic garnet peridotite (DR03-10, Fig. 2A) is the most common of the garnet ultramafic lithologies. Crystals of pink garnet, up to 2 cm in diameter, are the most conspicuous feature. The crystals are anhedral, but crudely equidimensional. The garnet contains fine (<1.5 mm) inclusions of transparent, emerald-green spinel. Locally, on a sub–cm scale, where olivine is absent (DR00-3), the garnet may also contain fine (<1 mm) inclusions of corundum. Magnesiohornblende occupies cracks and fractures in the garnet, and also forms light grey-green "kelyphitic" rims on the garnet. The kelyphite also occupies deep embayments in the garnet, and locally replaces garnet completely. In thin section, the kelyphitic magnesiohornblende resolves into pale green, fine- to medium-grained (1–2 mm) euhedral to subhedral crystals.

Clinopyroxene forms large (~6 mm), subhedral, generally rounded, crystals. Clinopyroxene does not contain inclusions of spinel. Crystals of clinopyroxene are rimmed by kelyphitic magnesiohornblende.

Partially serpentinized olivine forms a continuous, black matrix. In thin section (Fig. 2A), this matrix resolves into a fractured mosaic texture, with serpentine filling the late fractures. The olivine itself is free of inclusions.

Magnesiohornblende and serpentine are interpreted as the products of retrograde hydration. The original assemblage was Grt + Cpx + Ol + Spl, and locally, on a sub–cm scale where olivine is absent, Grt + Cpx + Spl + Crn.

Corundum-bearing garnet clinopyroxenite

The Corundum-bearing garnet clinopyroxenite (DR03-12) occurs as cm- to dm-scale irregular, cross-cutting veins in boulders of garnet clinopyroxenite (Abbott et al., 2003a, 2003b, 2005a). Large euhedral to subhedral crystals of clinopyroxene (up to 3 cm) form an orthocumulate texture (Fig. 2B). The interstices are filled by garnet. Spinel and corundum occur as fine (<1 mm) inclusions in garnet. Hornblende forms thin (1 mm) selvedges on the clinopyroxene. The hornblende is interpreted as the product of late, retrograde hydration. The original assemblage was Cpx + Grt + Spl + Crn. The orthocumulate texture serves as *prima facie* evidence of a magmatic origin, and the magmatic assemblages indicate asthenospheric conditions (P>3.4 GPa, T>1550°C; Abbott et al., 2003a, 2005a, 2005b).

Partially retrograde eclogite

Partially retrograded eclogite is fairly common in the garnet hornblende gneiss (Kc2). Foliation is developed weakly to strongly, depending on the amount of hornblende. The sample described here (DR03-7, Fig. 2C) is typical. Euhedral to subhedral porphyroblasts (1–3 mm) of pink garnet are evenly distributed in a matrix of symplectic intergrowth of micron-scale plagioclase and diopside. Garnet has sub–mm-scale inclusions of quartz and zoisite. Hornblende forms 0.2–0.5 mm thick rims on garnet, and also fills fracture in garnet. Fine (~0.1 mm) grains of hornblende and quartz are sparingly distributed in the symplectite matrix. Crystals of hornblende cut the fabric of the symplectite.

The symplectic intergrowth of plagioclase and diopside is interpreted as the product of the retrograde breakdown of original omphacite. Hornblende and zoisite are interpreted as the products of late, retrograde hydration. The assemblage at the highest grade of metamorphism was Omp + Grt + Qtz.

Mineral Analyses

Analytical techniques

Chemical analyses of minerals in garnet peridotite (Table 1), Crn-bearing garnet clinopyroxenite (Table 2), and eclogite (Table 3) were performed at the College of Arts and Sciences Microscope Facility, Appalachian State University. The instrument is an FEI Quanta 200 scanning electron microscope, fitted with an EDX microanalyzer (EDAX). Raw data were processed with Genesis 3.5 software. The analyses involved mineral standards furnished by the Smithsonian Institution (USNM series). The Genesis software has certain deficiencies with respect to constraints on the ZAF algorithm. The software does not provide for using more than one standard at a time, and the sum of the weight percents of oxides is constrained to 100. For the purpose of major-element analyses, these deficiencies were circumvented satisfactorily by proper choice of a standard, and by paying special attention to stoichiometry (i.e., atomic proportions of cations). No one standard is suitable for all purposes. In the garnet peridotite (DR03-10, DR00-3), USNM garnet standard (#110752) was used for analyzing garnet, spinel, and olivine. Confidence in the analyses is supported by comparison with analyses performed independently on some of the same minerals at the Florida Center for Analytical Microscopy, Florida

TABLE 1. Garnet Peridotite[1]

	Garnet peridotite, DR03-10b									Garnet peridotite, DR00-3			
Mineral:	Grt rim	Grt (FIU)[2]	Grt core	Spl core	Spl rim	Oli	Oli (FIU)	Cpx (FIU)[3]	Hbl (FIU)[4]	Grt	Spl	Grt	Spl
ID nos:.	1–5		6–10	1–11	12–14	1–5				1–17	1–10	18- 27	11–16
No. of analyses:	5	4	5	11	3	5	5	22	5	17	10	10	6
	wt%									wt%			
MgO	10.24	9.47	8.06	16.63	16.27	39.15	40.12	15.49	16.48	8.85	16.04	8.11	16.29
Al_2O^3	22.34	22.57	22.49	62.98	63.22	0.68	0.03	2.47	11.40	23.12	63.31	23.12	63.01
SiO_2	39.4	38.86	39.08	0.48	0.49	38.28	37.62	50.90	46.95	39.35	0.67	39.67	1.12
CaO	9.01	8.57	12.72	0.31	0.24	0.35	0.01	23.05	12.48	12.61	0.46	13.24	0.63
TiO_2	0.12	0.01	0.16	0.13	0.13	0.15	0.00	0.19	0.48	0.14	0.15	0.14	0.12
MnO	0.27	0.81	0.26	0.10	0.1	0.16	0.23	0.15	0.05	0.25	0.16	0.29	0.15
FeO	18.63	21.10	17.23	19.37	19.54	21.23	23.21	5.29	7.09	15.68	19.21	15.43	18.69
Total	100	101.40	100	100	100	100	101.27	97.76	96.99	100	100	100	100
	Cations p.f.u									Cations p.f.u			
Mg	1.15	1.05	0.91	0.64	0.63	1.51	1.53	0.87	3.51	0.99	0.62	0.91	0.63
Al	1.98	1.99	2.00	1.92	1.93	0.02	0.00	0.13	1.92	2.04	1.93	2.05	1.92
Si	2.96	2.90	2.95	0.01	0.01	0.99	0.96	1.90	6.72	2.95	0.02	2.98	0.03
Ca	0.73	0.69	1.03	0.01	0.01	0.01	0.00	0.93	1.91	1.01	0.01	1.07	0.02
Ti	0.01	0.00	0.01	0.00	0.00	0.00	0.00	0.01	0.05	0.01	0.00	0.01	0.00
Mn	0.02	0.05	0.02	0.00	0.00	0.00	0.00	0.00	0.01	0.02	0.00	0.02	0.00
Fe	1.17	1.32	1.09	0.42	0.42	0.46	0.49	0.16	0.85	0.98	0.42	0.97	0.40
Total	8.00	8.00	8.00	3.00	3.00	3.00	3.00	4.0	15.45	8.00	3.00	8.00	3.00
												0.00	
Q[5]	23.91	23.79	23.92	7.95	7.96	8.00	7.88	11.94		23.96	7.97	24.03	7.98
Fe‴	0.09	0.21	0.08	0.05	0.04	0.00	0.12	0.06		0.04	0.03	0.00	0.02
Fe″	1.08	1.11	1.01	0.36	0.38	0.46	0.37	0.10		0.94	0.38	0.97	0.38
Mg#	0.49	0.49	0.45	0.60	0.60	0.77	0.78	0.84	0.81	0.50	0.60	0.48	0.61
prp	0.37	0.36	0.30							0.33		0.31	
grs	0.24	0.24	0.34							0.34		0.36	
alm	0.38	0.38	0.36							0.33		0.33	
spl				0.64	0.63						0.62		0.63
hc				0.34	0.36						0.35		0.36
mag				0.03	0.02						0.02		0.01
wo								0.47					
en								0.44					
fs								0.08					
jd								0.01					

[1]Garnet standard #5 (NBS 110752)

[2]FIU = analyses performed at Florida Center for Analytical Electron Microscopy, Florida International University; Abbott et al., 2001a, 2005a, 2005b.

[3]Cpx (FIU) includes Na_2O = 0.12 wt.% (Na = 0.01 pfu).

[4]Hbl (FIU) = includes Na_2O = 1.49 wt% (Na = 0.41 pfu).

[5]Q = sum of cation charges.

TABLE 2. Mineral Analyses, Garnet Clinopyroxenite, DR03-12[1]

Mineral:	Grt rim	Spl	Grt core	Grt cr-rm	Grt rim	Spl core	Spl rim	Cpx
ID nos.:	1–5	1–4	11–15	16–18	6–10	10–15	5–9, 16–17	1–19
No. of analyses:	5	4	5	3	5	6	7	17
				wt%				
Na_2O	n.a.	n.a.	n.a.	n.a.	n.a.	n.a.	n.a.	0.65
MgO	6.97	9.48	2.54	6.51	8.31	10.60	10.85	16.99
Al_2O_3	21.83	57.65	21.83	21.77	21.81	59.91	59.95	1.56
SiO_2	38.90	0.63	38.62	38.36	39.42	0.30	0.28	52.11
K_2O	n.a.	n.a.	n.a.	n.a.	n.a.	n.a.	n.a.	0.05
CaO	11.13	0.34	16.26	12.51	9.67	0.32	0.30	24.38
TiO_2	0.13	0.10	0.13	0.09	0.15	0.18	0.16	0.31
MnO	0.71	0.27	1.59	0.77	0.64	0.27	0.29	0.11
FeO	20.33	31.55	19.03	19.98	19.99	28.43	28.18	3.85
Total	100	100	100	100	100	100	100	100
				Cations p.f.u				
Na	–	–	–	–	–	–	–	0.05
Mg	0.79	0.39	0.29	0.74	0.94	0.43	0.43	0.92
Al	1.97	1.86	2.00	1.96	1.95	1.91	1.91	0.07
Si	2.97	0.02	3.00	2.93	3.00	0.01	0.01	1.89
K	–	–	–	–	–	–	–	0.00
Ca	0.91	0.01	1.35	1.03	0.79	0.01	0.01	0.95
Ti	0.01	0.00	0.01	0.01	0.01	0.00	0.00	0.01
Mn	0.05	0.01	0.10	0.05	0.04	0.01	0.01	0.00
Fe	1.30	0.72	1.24	1.28	1.27	0.64	0.63	0.12
Total	8.00	3.00	8.00	8.00	8.00	3.00	3.00	4.00
Q	23.93	7.90	24.02	23.84	23.96	7.93	7.93	11.82
Fe‴	0.07	0.10	0.00	0.16	0.04	0.07	0.07	
Fe″	1.23	0.62	1.24	1.12	1.23	0.57	0.56	
Mg#	0.38	0.35	0.19	0.37	0.43	0.40	0.41	0.89
prp	0.26		0.10	0.24	0.31			
grs	0.30		0.45	0.33	0.26			
alm	0.43		0.41	0.41	0.42			
spl		0.39				0.43	0.43	
hc		0.56				0.53	0.53	
mag		0.05				0.04	0.04	
wo								0.47
en								0.45
fs								0.06
jd								0.02

[1]Garnet standard #5 (NBS 110752) for Grt, Spl; Omphacite standard #9 (NBS 110607) for Cpx; n.a. = not analyzed.

International University (FIU analyses reported in Table 1). In the Crn-bearing clinopyroxenite (DR03-12), USNM garnet standard (#110752) was used for garnet and spinel; and USNM omphacite standard (#110607) was used for clinopyroxene. In the eclogite (DR03-7), USNM omphacite standard (#110607) was used for all minerals (hornblende, garnet, plagioclase and clinopyroxene).

Iron was reported as weight percent FeO. The weight percent oxide components were recalculated as atomic proportions of cations, normalized to 8 cations per formula unit (pfu) for garnet, 4 cations pfu for clinopyroxene, 3 cations pfu for spinel and olivine, 5 cations pfu for plagioclase, and 15 cations pfu for hornblende (excluding Na). Fe^{3+} was estimated on the basis of stoichiometry and charge balance.

Data

Minerals in two assemblages were analyzed for the garnet peridotite (Table 1). Minerals in sample DR03-10 refer to the assemblage Cpx + Ol + Grt + Spl + Mg-hornblende + serpentine. No analyses were performed on the serpentine. Minerals in sample DR00-3 refer to the assemblage Cpx + Grt + Spl + Crn + Mg-hornblende in a cm-scale, olivine-free part of the garnet peridotite. Garnet is not notably zoned (core, rim), and the composition is similar in both assemblages. The typical composition has more or less equal mole % of prp, alm, and grs components, and less than 1 mole % sps. Spinel compositions are remarkably uniform both within individual grains (core, rim) and from one grain to another, and essentially the same in both assemblages. The composition is $spl_{63}hc_{36}mag_{01}$.

Mineral analyses for the Crn-bearing garnet clinopyroxenite (DR03-12) refer to the assemblage Cpx + Grt + Spl + Crn + hornblende (Table 2). Garnet analyses show some variation, but this cannot be characterized well without more chemical analyses. Compared to the garnet peridotite, the garnet in the clinopyroxenite has less Mg (10–31 mole% prp), consistently more Fe (41–43 mole % alm), and similar, but more variable Ca (26–45 mole% grs). Spinel is uniform in composition, with notably less Mg (39–43 mole% spl) and more Fe (53–56 mole% hc, 4–5 mole% mag) than spinel in the garnet peridotite. The composition of the clinopyroxene ($wo_{47}en_{45}fs_{07}jd_{02}$) is the average of 17 single-point analyses, at 0.5 mm intervals along a traverse (rim to core to rim) across the phenocryst near the center of Figure 2B (nearly surrounded by garnet). Within reasonable limits of analytical uncertainty, the traverse showed no variation in any element across the phenocryst. The clinopyroxene has essentially the same composition as clinopyroxene in garnet peridotite (Table 1).

TABLE 3. Mineral Analyses, eclogite, DR03-7[1]

			Symplectite	
Mineral:	Hbl	Grt	Pla	Cpx
No. of analyses:	3	5	3	5
		wt%		
Na_2O	2.10	0.26	7.61	1.99
MgO	11.63	5.74	0.28	11.16
Al_2O_3	13.33	22.65	24.98	4.29
SiO_2	43.27	36.35	62.78	51.18
CaO	12.62	8.63	4.14	22.08
FeO	17.06	26.37	0.21	9.30
Total	100	100	100	100
		Cations p.f.u		
Na	0.59	0.04	0.66	0.14
Mg	2.50	0.66	0.02	0.62
Al	2.26	2.07	1.31	0.19
Si	6.23	2.81	2.80	1.89
Ca	1.95	0.72	0.20	0.88
Fe	2.06	1.71	0.01	0.29
Total	15.59	8.00	5.00	4.00
Q	45.32	23.65	16.26	11.83
Fe‴	0.68	0.35	0.00	0.17
Fe″	1.38	1.36	0.01	0.12
Mg#	0.64	0.33		0.84
Al(iv)	1.77		1.31	0.11
ts (8-Si-Na)	1.18			
ed (Na)	0.59			
ab			0.77	
an			0.23	
prp		0.21		
grs		0.23		
alm		0.55		
wo				0.44
en				0.31
fs				0.14
jd				0.07

[1]Omphacite standard #9, NBS 110607.

Chemical analyses of minerals in eclogite (DR03-7) are reported in Table 3. Compositions of the components of the symplectite are plagioclase $ab_{77}an_{23}$ and clinopyroxene $wo_{44}en_{31}fs_{14}jd_{07}$. The

TABLE 4. P-T Estimates

	Sample	Assemblage	P, GPa	T, °C			
		Thermobarometry, WEBINVEQ					
Grt peridotite	DR03-10	Grt-Cpx-Oli-Spl	4.15	867			
Grt peridotite	DR00-3	Grt-Cpx-Spl-Crn	3.00	838			
Grt clinopyroxenite	DR03-12	Grt-Cpx-Spl-Crn	2.75	807			
eclogite	DR03-7	Grt-Cpx-Pla-Qtz	1.76	731			
	Grt-Cpx at P = 1.5 GPa			Grt-Cpx at P = 3 GPa			Grt-Hbl
			Thermometry, T °C				
Ref.[1]	A(94)	K(98)	R(04)	A(94)	K(88)	R(00)	GP(84)
Grt peridotite	751	637	599	849	679	673	664
Grt clinopyroxenite	771	651	595	858	689	663	732
Eclogite	690	624	538	782	664	609	727

[1]A(94) = Ai, 1994; K(88) = Krogh, 1988; R(00) = Ravna, 2000; GP(84) = Graham and Powell, 1984.

garnet composition ($prp_{21}grs_{23}alm_{55}$) pertains to the edge of a porphyroblast next to symplectic intergrowth of plagioclase and clinopyroxene. The hornblende analyses are from a 0.5 mm wide rim formed on a garnet porphyroblast.

P-T Estimates

The garnet peridotite and garnet clinopyroxenite originated as igneous rocks in the asthenosphere (Abbott et al., 2003b, 2005a). The mineral assemblages constrain the magmatic conditions to P > 3.4 GPa and T > 1550°C. Previously estimated P-T conditions based on mineral equilibrium show that the minerals reequilibrated under subsolidus conditions, P = 2.8–3.4 GPa and T = 740-810°C (Abbott et al., 2003b, 2005a). These subsolidus conditions were based on a limited number of chemical analyses of minerals, and chemical analyses of the spinel were of questionable accuracy. New chemical analyses, presented here, provide for much-improved estimates of the subsolidus P-T conditions of the garnet ultramafic rocks, and provide for an estimate of the P-T conditions for the associated eclogite.

P and T were estimated by two means: (1) multiple-equilibrium analysis (WEBINVEQ; Gordon, 1999) and (2) Fe-Mg exchange thermometry involving pairs of minerals, Grt-Cpx and Grt-Hbl. Results are reported in Table 4, and portrayed in Figure 3.

WEBINVEQ

Starting with the mineral analyses, the activities of end member components of minerals in an assemblage were calculated using the program AX, written by Holland and Powell (2000). The activities were converted to single-site mixing models and then entered, online, into the program WEBINVEQ, developed by Gordon (1999). WEBINVEQ determines the equilibrium conditions for all possible equilibria involving the mineral components. Each such equilibrium describes a line in P-T space. Ideally the lines for all such equilibria would intersect at P-T conditions satisfying all of the equilibria. Typically the equilibria do not intersect at a well-defined point, in which case a search is conducted for the set of activities that gives the best solution. The results provide for error analysis, and assessment of uncertainty in the estimated conditions. Ellipses in Figure 3 represent 68.3% confidence, assuming an error of ±1 kJ for the chemical potential of each mineral component.

Estimated equilibrium P-T conditions for the assemblage Grt + Cpx + Oli + Spl in garnet peridotite are 4.15 GPa, 867°C (Fig. 3). Estimated equilibrium conditions for the assemblage Grt + Cpx + Spl + Crn in garnet peridotite and garnet clinopyroxene are similar, 3.00 GPa, 838°C, and 2.75 GPa, 807°C, respectively. Equilibrium conditions for the assemblage Grt + Cpx + Pl + Qtz in eclogite are 1.76 GPa,

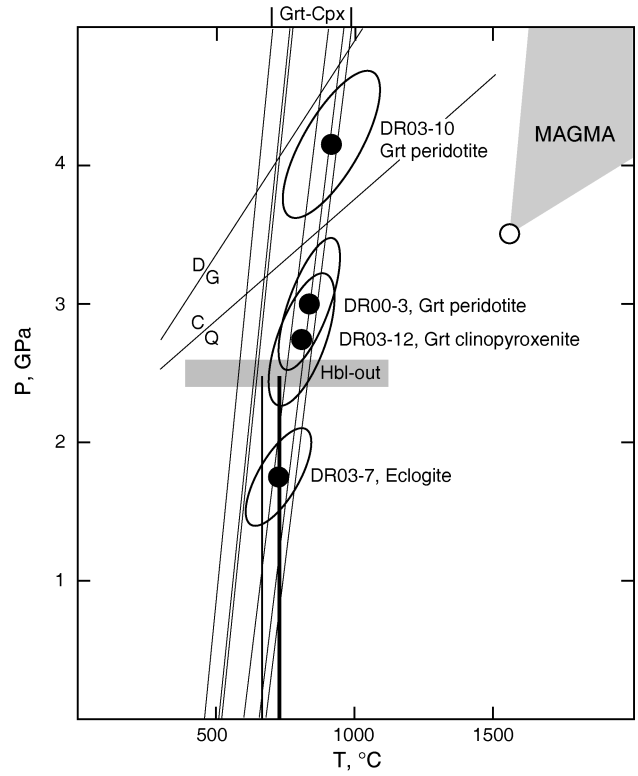

FIG. 3. Estimated P-T conditions. The shaded region (P > 3.5 GPa, T > 1550°C) defines the magmatic conditions for the garnet ultramafic rocks. Filled circles represent results of WEBINVEQ calculations. The ellipses represent 68.3 % confidence, assuming ±1 kJ error in the chemical potential of each mineral component. Results of Cpx-Grt thermometry are represented by the steep fine lines. Results of Grt-Hbl thermometry are represented by the fine vertical lines, terminating at about 2.5 GPa, the approximate upper pressure limit for hornblende. Abbreviations: D/G = diamond-graphite; C/Q = coesite-quartz.

731°C, and relate to the decomposition of omphacite to plagioclase + diopsidic clinoproxene. The four WEBINVEQ P-T conditions fall essentially on a single line of steep P-T slope (Fig. 3).

Fe-Mg exchange thermometry

Temperatures were calculated at two pressures (1.5 GPa, 3.0 GPa) for three models of Fe-Mg exchange between garnet and clinopyroxene (Ai, 1994; Krogh, 1988; Ravna, 2000). The relative merits of these and other models are discussed in Ravna and Paquin (2003). Other models, notably Pattison and Newton (1989), give anomalously low temperatures (Ravna and Paquin, 2003) for these rocks. In Figure 3, only the maximum (Ai, 1994) and minimum (Ravna, 2000) Grt-Cpx temperatures are shown for each mineral assemblage. Ai's (1994) Grt-Cpx model agrees most closely with the WEBINVEQ conditions.

Temperatures were also calculated for Fe-Mg exchange between garnet and hornblende, using the model of Graham and Powell (1984). Results are shown in Figure 3 as the vertical lines terminating at about 2.5 GPa, the approximate upper pressure limit for hornblende (Gilbert et al., 1982; Poli and Fumagali, 2003). At P < 2.5 GPa, the Grt-Hbl temperatures are consistent with temperatures from Ai's (1994) model for Grt-Cpx, suggesting that garnet, clinopyroxene, and hornblende were in equilibrium at P < 2.5 GPa. Of course, this does not preclude that garnet and clinopyroxene were also in equilibrium at higher pressures, consistent with the WEBINVEQ estimates for the garnet ultramafic rocks. As noted, there is good evidence that the garnet ultra-

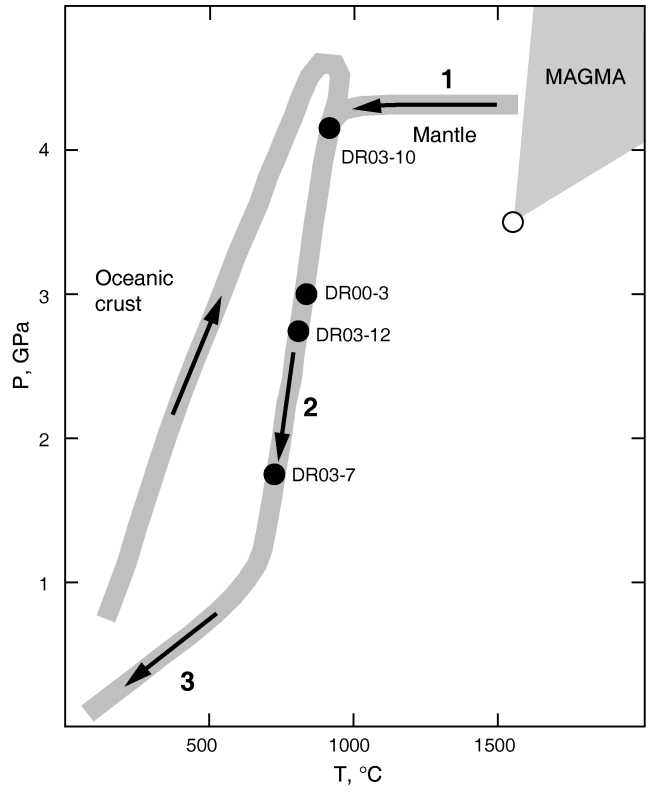

FIG. 4. Proposed P-T paths for garnet ultramafic rocks (1, 2, 3), and for oceanic crust (eclogite). Results of WEBINVEQ calculations are shown as filled circles.

mafic rocks originated at very high pressures, well above the upper pressure limit for hornblende (Abbott et al., 2003b, 2005a).

P-T Paths

Figure 4 illustrates inferred P-T paths for the garnet ultramafic rocks and for the associated eclogite. The P-T path for the garnet ultramafic rocks is modeled in three parts, starting from solidus conditions, >1550°C, > 3.4 GPa (Abbott et al., 2003b, 2005a).

1. Slow, approximately isobaric (~4 GPa) cooling in the mantle, down to approximately 850°C. No signature of magmatic conditions is preserved in the major-element chemistry of the minerals. The lack of chemical zoning in garnet and clinopyroxene crystal requires a very slow cooling rate for complete reequilibration of the mineral chemistry in the large (cm-scale) crystals. The conditions (4.15 GPa, 867°C, Table 3) are similar to those estimated for other garnet peridotite bodies in UHP terranes in China, Indonesia, Scandinavia, and the Alpine-Carpathian system (Medaris, 1999).

2. Relatively rapid, nearly adiabatic(?) decompression, ~4 GPa (~850°C) down to ~1 GPa (~700°C). The preservation of the mineral chemistries consistent with UHP conditions and steepness of the P-T path suggests rapid uplift. This part of the path compares well with decompression paths for other UHP rocks (e.g., Carswell and Zhang, 1999).

3. Relatively rapid, non-adiabatic decompression and cooling. H_2O entering and passing through the system in the formation of hornblende and serpentine would enhance heat loss through hydrothermal fluid convection, hence increasing the rate of cooling.

P-T conditions for the eclogite fall on the second part of the path. Field observations indicate that the garnet ultramafic rocks are meter-scale pods in the

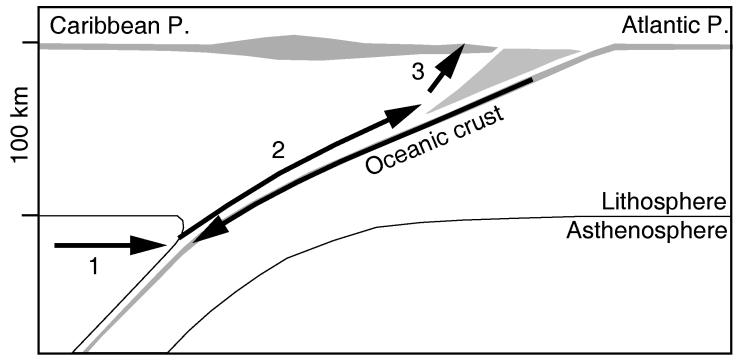

FIG. 5. Simplified plate tectonic interpretation. Three parts of the P-T path for the garnet ultramafic rocks are numbered (1, 2, 3) as in Figure 4. Eclogite originated as oceanic crust.

eclogite, and as such must have been delivered to the surface in the eclogite. An oceanic crustal origin for the hornblende schist and gneiss of the Cuaba Gneiss indicates that the early history of the greater part of the Cuaba Gneiss was independent of the early history of the garnet ultramafic rocks. The hypothetical P-T path shown in Figure 4 for the early history of the eclogite is admittedly poorly constrained, and meant only to be consistent with current models for deep-subduction of oceanic crust (e.g., Gerya et al., 2002; Roselle and Engi, 2002; Roselle et al., 2002; Gerya and Yuen, 2003).

Conclusions

Figure 5 offers a bare-bones tectonic interpretation. The isobaric part of the P-T path for the garnet ultramafic rocks (1, Fig. 4) took place in the mantle and relates to delivery of the rocks to deep-subducted oceanic crust in mid- to Late Cretaceous time. Garnet ultramafic rocks of the mantle wedge and deep-subducted oceanic crust were juxtaposed, and the former cooled, in response to erosion of the hanging wall of the subduction zone. Alternatively (not illustrated in Fig. 5), the process may have taken place during initiation of subduction, in which case the garnet ultramafic rocks may have been incorporated, and cooled, at the leading edge of the downgoing oceanic crust. In either case, incorporation of Grt ultramafic rocks in the deep-subducted oceanic crust (eclogite) marked the end of the first part of the path. The second part of the P-T path (2, Fig. 4) was associated with transport up the subduction zone, perhaps by reverse flow, as modeled by Gerya et al. (2002) and Gerya and Yuen (2003). This stage was essentially completed prior to mid-crustal intrusion by dioritic to gabbroic rocks (Rio Boba Complex) of uncertain, but presumably Late Cretaceous, age. The third part of the path (3, Fig. 4) relates to final uplift to the surface, completed by mid-Eocene time, perhaps in response to initiation of transcurrent tectonics (Mann et al., 1990; Pindell and Barrett, 1990; Draper et al., 1994, 1996; Pindell, 1994; Pindell et al., 2005).

Acknowledgments

The project is supported by National Science Foundation Grants EAR-8306145, EAR-8509542, and INT-0139536 to Draper and NSF Grants EAR-0111471 and INT-0139490 to Abbott. The research was supported by an Appalachian State University Research Grant to Abbott. We especially appreciate the assistance and patience of Dr. Ruth Dewel, Director, College of Arts and Sciences Microscope Facility, Appalachian State University.

REFERENCES

Abbott, R. N., Jr., and Draper, G., 1998, Retrograde eclogite in the Cuaba Amphibolite of the Rio San Juan Complex, northern Hispaniola, *in* 15th Caribbean Geological Conference, Kingston, Jamaica.

Abbott, R. N., Jr., and Draper, G., 2002, Retrograded eclogite in the Cuaba Amphibolite of the Rio San Juan Complex, Northern Hispaniola, *in* Jackson, T. A., ed., Caribbean geology: Into the third millennium: Transactions of the 15th Caribbean Geological Conference: Kingston, Jamaica, The University of the West Indies Press, p. 97–108.

Abbott, R. N., Jr., Draper, G., and Keshav, S., 2001a, Garnet peridotite found in the Greater Antilles: EOS (Transactions of the American Geophysical Union), v. 82, no. 35, p. 381–388.

Abbott, R. N., Jr., Draper, G., and Keshav, S., 2001b, Alpine-type garnet peridotite in the Caribbean [abs.]: Geological Society of America Abstracts with Programs, v. 33, no. 6, Boston.

Abbott, R. N., Jr., Draper, G., and Keshav, S., 2003a, Tectonic implications of UHP garnet peridotite in the Cuaba Unit, Rio San Juan Complex, Dominican Republic [abs.]: Geological Society of America Abstracts with Programs, v. 35, no. 2, Puerta Vallarta.

Abbott, R.N., Jr., Draper, G., and Keshav, S., 2003b, UHP magmatic paragenesis, garnet peridotite, Cuaba Unit, Rio San Juan Complex, Dominican Republic [abs.]: Geological Society of America Abstracts with Programs, v. 35, no. 6, Seattle.

Abbott, R. N., Jr., Draper, G., and Keshav, S., 2005a, UHP magma paragenesis, garnet peridotite, and garnet clinopyroxenite: An example from the Dominican Republic. International Geology Review, v. 47, 233–247.

Abbott, R. N., Jr., Draper, G., and Keshav, S., 2005b, UHP metamorphism in garnet peridotite, Cuaba unit, Rio San Juan complex, Dominican Republic, *in* Draper, G., ed., Transactions of the 16th Caribbean Geological Conference, Barbados: Caribbean Journal of Earth Science, v. 39, p. 13–20.

Ackermand, D., Seifert, F., and Schreyer, W., 1975, Instability of sapphirine at high pressures: Contributions to Mineralogy and Petrology, v. 50, p. 79–92.

Ai, Y., 1994, A revision of the garnet-clinopyroxene Fe^{2+}-Mg exchange geothermometer: Contributions to Mineralogy and Petrology, v. 115, p. 467–473.

Broman, B. N., Abbott, R. N., Jr., and Draper, G., 2005, P-T path for UHP garnet ultramafic rocks, Cuaba Gneiss, Rio San Juan Complex, Dominican Republic: Geological Society of America Abstracts with Programs, v. 37, no. 6, Salt Lake City.

Carswell, D. A., and Zhang, R. G., 1999, Petrographic characteristics and metamorphic evolution of ultrahigh-pressure eclogites in plate-collision belts: International Geology Review, v. 41, p. 781–798.

Draper, G., Abbott, R. N., Jr., and Keshav, S., 2002, Indication of UHP metamorphism in garnet peridotite, Cuaba Unit, Rio San Juan Complex, Dominican Republic: Sixteenth Caribbean Geological Conference, Barbados.

Draper, G., Gutierrez, G., and Lewis, J. F., 1996, Thrust emplacement of the Hispaniola peridotite belt: Orogenic expression of the mid-Cretaceous Caribbean arc polarity reversal?: Geology, v. 24, p. 1143–1146.

Draper, G., Mann, P., and Lewis, J. F., 1994, Hispaniola, *in* Donovan, S. K., and Jackson, T. A., 1994, eds., Caribbean geology: An introduction: Kingston, Jamaica, University of the West Indies Press, p. 129–150.

Draper, G., and Nagle, F., 1991, Geology, structure, and tectonic development of the Rio San Juan Complex, northern Dominican Republic, *in* Mann, P., Draper, G., and Lewis, J. F., eds., Geologic and Tectonic development of the North American–Caribbean plate boundary in Hispaniola: Geological Society of America Special Paper 262, p. 77–95.

Eberle, W., Hirdes, W., Muff, R., and Pelaez, M., 1982, The geology of the Cordillera Septentrional (Dominican Republic), *in* Snow, W., Gil, N., Llinas, R., Rodriguez-Torres, R., and Tavares, I., eds., Transactions, 9th Caribbean Geological Conference, Santo Domingo, Dominican Republic, 1980, p. 619–632.

Gerya, T. V., Stockert, B., and Perchuk, A. L., 2002, Exhumation of high-pressure metamorphic rocks in a subduction channel: A numerical simulation: Tectonics, v. 21, 6-6, 1056 [doi:10.1029/2002TC001406].

Gerya, T. V., and Yuen, D. A., 2003, Rayleigh-Taylor instabilities from hydration and melting propel 'cold plumes' at subduction zones: Earth and Planetary Science Letters, v. 212, p. 47–62.

Gilbert, M. C., Heltz, R. T., Popp, R. K., and Spear, F. S., 1982, Experimental studies of amphibole stability, *in* Veblen, D. R., and Ribbe, P. H., eds., Amphiboles: Petrology and experimental phase relationships: Reviews in Mineralogy, v. 9B, p. 229–354.

Gordon, T., 1999, Generalized thermobarometry: WEBINVEQ with the TWQ 1.02 data base [http://ichor.geo.ucalgary.ca/~tmg/Webinveq/rgb95.html].

Graham, C. M., and Powell, R., 1984, A garnet-hornblende geothermometer: Calibration, testing, and application to the Pelona Schist, Southern California: Journal of Metamorphic Geology, v. 2, p. 13–21.

Holland, T. J.B., and Powell, R., 2000, AX, Mineral activity calculation for thermobarometry: Cambridge, UK, Cambridge University, computer program AX2, v. 2.2.

Jansma, P. E., Mattioli, G. S., Lopez, A., DeMets, C., Dixon, T. H., Mann, P., and Calais, E., 2000, Neotectonics of Puerto Rico and the Virgin Islands, northeastern Caribbean, from GPS geodesy: Tectonics, v. 19, p. 1021–1037.

Kretz, R., 1983, Symbols for rock-forming minerals: American Mineralogist, v. 68, p. 277–279.

Krogh, E. J., 1988, The garnet-clinopyroxene Fe-Mg geothermometer—a reinterpretation of existing experimental data: Contributions to Mineralogy and Petrology, v. 99, p. 44–48.

Lewis, J. F., and Draper, G., 1990, Geology and tectonic evolution of the northern Caribbean region, *in* Dengo, G., and Case, J. E., eds., The Caribbean region: Boulder, CO, Geological Society of America, Geology of North America, v. H, p. 77–140.

Mann, P., Calais, E., Ruegg, J.-C., DeMets, C., Jansma, P. E., and Mattioli, G. S., 2002, Oblique collision in the northeastern Caribbean from GPS measurements and geological observations: Tectonics, v. 21, no. 6-7, 1057 [doi:10.1029/2001TC001304].

Mann, P., Schubert, C., and Burke, K., 1990, Review of Caribbean neotectonics, *in* Dengo, G., and Case, J. E., eds., The Caribbean Region: Boulder, CO, Geological Society of America, Geology of North America, v. H, p. 307–338.

Medaris, L. G., Jr., 1999, Garnet peridotites in Eurasian high-pressure and ultrahigh-pressure terranes: A diversity of origins and thermal histories: International Geology Review, v. 41, p. 799–815.

Pattison, D., and Newton, R. C., 1989, Reversed experimental calibration of the garnet-clinopyroxene Fe-Mg exchange thermometer: Contributions to Mineralogy and Petrology, v. 101, p. 87–103.

Pindell, J. L., 1994, Evolution of the Gulf of Mexico and the Caribbean, *in* Donovan, S. K., and Jackson, T. A., eds., Caribbean geology: An introduction: Kingston, Jamaica, University of the West Indies Press, p. 13–19.

Pindell, J. L., and Barrett, S. F., 1990, Geological evolution of the Caribbean region: A plate tectonic perspective, *in* Dengo, G., and Case, J. E., eds., The Caribbean region: Boulder, CO, Geological Society of America, Geology of North America, v. H, p. 405–432.

Pindell, J. L., Kennan, L., Maresch, W. V., Stanek, K-P., Draper, G., and Higgs, R., 2005, Plate-kinematics and crustal dynamics of circum-Caribbean arc-continent interactions and tectonic controls on basin development, *in* Ave Lallemant, H. G., and Sisson, V. B., eds., Proto-Caribbean margins in Caribbean–South American plate interactions, Venezuela: Geological Society of America Special Paper 394, p. 7–52.

Poli, S., and Fumagali, P., 2003, Mineral assemblages in ultrahigh pressure metamorphism: A review of experimentally determined phase diagrams, *in* Carswell, D. A., and Compagnoni, R., eds., Ultrahigh pressure metamorphism: EMU Notes in Mineralogy, v. 5, p. 307–340.

Ravna, E., 2000, The garnet-clinopyroxene geothermometer: An updated calibration: Journal of Metamorphic Geology, v. 18, p. 211–219.

Ravna, E., and Paquin, J., 2003, Thermobarometric methodologies applicable to eclogites and garnet ultrabasites, *in* Carswell, D. A., and Compagnoni, R., eds., Ultrahigh pressure metamorphism: EMU Notes in Mineralogy, v. 5, p. 229–259.

Roselle, G. T., and Engi, M., 2002, Ultra high pressure (UHP) terrains: Lessons from thermal modeling: American Journal of Science, v. 302, p. 410–441.

Roselle, G. T., Thuring M., and Engi, M., 2002, MELONPIT: A finite element code for simulating tectonic mass movement and heat flow within subductions zone: American Journal of Science, v. 302, p. 381–409.